energies

Article

Research on Non-Contact Voltage Measurement Method Based on Near-End Electric Field Inversion

Shangpeng Sun [1], Feiyue Ma [1], Qing Yang [2,*], Hui Ni [1], Tao Bai [3], Kun Ke [2] and Zhenhui Qiu [2]

1 Electric Power Research Institute of Ningxia Electric Power Co., Ltd., Yinchuan 750001, China; sunshangpeng@dky.nx.sgcc.com.cn (S.S.)
2 State Key Laboratory of Power Transmission Equipment and System Security and New Technology, Chongqing University, Chongqing 400044, China
3 State Grid Ningxia Electric Power Co., Ltd. Shizuishan Power Supply Company, Shizuishan 753000, China
* Correspondence: yangqing@cqu.edu.cn

Abstract: Aiming at the problems of complex equations, low accuracy, and the strict measurement point layout requirements of the existing electric field integration method, a non-contact measurement method based on the inversion voltage of the near electric field is proposed. Firstly, the field source relationship is clarified, the connection between the spatial electric field and the voltage is derived, and a near-end electric field inversion method is proposed. Secondly, a three-dimensional simulation model of an overhead line is established using COMSOL finite element software, the three-dimensional spatial potential distribution of the overhead line is obtained, and the voltage is inverted and calculated. Finally, an overhead line simulation test platform was built, and MEMS electric field sensors were used for testing and verification. The results show that the maximum error of the three-phase voltage inversion of the proximal electric field measurement is 6.8%, and the error between the voltage obtained by the experimental inversion measurement and the reference voltage is less than 7.2%. The simulation and experimental results also verify the accuracy and feasibility of the inversion voltage of the proximal electric field. The results of this paper can lay a foundation for the practical application of small and miniaturized electric field sensors, and help in the construction and development of smart grids.

Keywords: overhead lines; proximal electric field measurement; contactless; voltage inversion

Citation: Sun, S.; Ma, F.; Yang, Q.; Ni, H.; Bai, T.; Ke, K.; Qiu, Z. Research on Non-Contact Voltage Measurement Method Based on Near-End Electric Field Inversion. *Energies* **2023**, *16*, 6468. https://doi.org/10.3390/en16186468

Academic Editor: Krzysztof Górecki

Received: 29 July 2023
Revised: 30 August 2023
Accepted: 31 August 2023
Published: 7 September 2023

Correction Statement: This article has been republished with a minor change. The change does not affect the scientific content of the article and further details are available within the backmatter of the website version of this article.

1. Introduction

With the rapid development of the economy and society, the scale of smart grids is expanding. As a result, the ecology of the power system is also changing profoundly, and improving the holographic sensing ability of power equipment is an important means of ensuring the safe and stable operation of the power grid [1,2]. Grid monitoring mainly includes the two categories of electrical and non-electrical quantities. Among these, voltage is one of the most basic electrical quantities that can directly reflect the operating status of power equipment and fault information [3,4]. Therefore, obtaining high-precision voltage data is of great significance for the construction of a new type of safe and efficient power system. Compared with the traditional measurement method, non-contact voltage measurement technology has higher safety due to the lack of direct electrical connection, and the sensing device has the advantages of having a small size and cheap cost, and can meet the measurement needs of a wide range of layouts [5–7]. Currently, the sensor element and inverse measurement principle are the two key issues constraining non-contact voltage measurement. Non-intrusive voltage measurement can be realized via the current use of advanced MEMS (Micro Electro Mechanical Systems) technology [7], the optical principle [8], the electrostatic induction principle [9], and other methods to develop sensors that measure the electric field distribution in the space around the conductor. Compared with existing contact voltage sensors are based on the principle of electric field coupling or the stray capacitance voltage divider. The non-contact measurement not only avoids the impact of the environment on the stray capacitance, but also realizes the electric field decoupling under condition of the multi-source conductors [10]. In addition, the corresponding sensor is also a good choice for the realization of electric field inversion measurement. The sensor also provides the basis for a device that realizes the electric field inversion voltage. Therefore, in recent years, determining how to utilize the electric field as an indirect parameter for voltage inversion has received extensive attention from scholars at home and abroad, and has gradually become a popular research issue.

The current technical means of inverting the voltage by measuring the electric field can be divided into the electric field inverse problem-solving method and the electric field integration method according to the principle used. The electric field inverse problem method is used to calculate the conductor voltage based on the information and boundary conditions of the electric field in the space around the conductor being measured. Based on the improved simulated charge method, He Wei's research team at Chongqing University arranged a certain number of electric field measurement points in the area near the insulator, and calculated the inverse problem of the insulator electric field through the acquired electric field information, thereby determining the presence or absence of poor-quality insulators. However, the solution process needs to deal with the inverse problem arising from the measurement error and interference unsuitability [11,12]. Based on the analysis of the "field-source-sense" positive and negative problems, and through the electric field measurement and voltage inversion of the charged line, Wang's research team realized the positive problem solving and inverse problem validation of various charge models; however, there are still difficulties and pathological problems in the solving process [13–17]. Xiao Dongping's research team proposed improvement measures based on the particle swarm algorithm and worm algorithm for the abnormalities of electric field inverse problem solving [18,19]. Based on the PT (Potential Transformer) low-frequency core saturation problem, the team proposed an inverse mathematical model with nonlinear components and a calculation method through the electromagnetic dyadic π model, which greatly reduces the measurement error of the PT excitation voltage [20]. The inverse problem solving involves complex matrix inverse operations, which leads to the problems of long computation time, low efficiency, and abnormalities. Moreover, there are differences between the field and theoretical field source models, so the electric field inverse problem-solving method is difficult to use in the field. The electric field integration method is a solution method that calculates the voltage of the measured conductor with the help of numerical integration via the measurement of the electric field information at multiple points on the electric field line from the ground potential to the measured conductor. The Canadian scholars Rahmatian F and Chavez P.P. et al. successfully introduced the numerical integration method into voltage measurement by using three electric field sensors arranged in their positions according to the orthogonal method to obtain the electric field information. The accuracy of the method was tested via practical calculations and the voltage inversion results maintained an accuracy of 0.2% in both normal measurements and in the presence of disturbances in the electric field [21]. The Canadian scholars Chavez. P.P. and Jaeger N. et al. proposed that only two electric field sensors can be used to design an accurate voltage integral inversion device, which does not have the problem of equipment insulation and shielding [22]. Zhu Yong et al. of Huazhong University of Science and Technology proposed a measurement method for optical path integration of a 220 kV high-voltage electric field and direct measurement of grid voltage to overcome the shortcomings of electric fields that are susceptible to perturbation. However, the selection scheme of the integration node of this method is relatively vague, and the accuracy of the experimental results has to be further studied [23]. Wang Jinguang's research team proposed applying the integration method to the measurement of energized lines by arranging multiple D-dot electric field sensors on the lines' plumb line and using a Gauss-type integration method with fixed nodes for line voltage measurement. Although they effectively optimized the placement of the electric field sensors under the premise of ensuring the accuracy of voltage inversion, it is still difficult to install some of the sensor nodes in the field [24–26]. Although the existing electric field integral method avoids the complex matrix calculation and abnormality problems in the solution of the electric field inverse problem, the method requires the arrangement of multiple electric field sensors on the electric field line from the ground potential to the measurement conductor, and there is still the problem of unclear selection of the reference ground potential at this stage. Therefore, although the integral method of measurement is theoretically feasible, it is difficult to apply it considering the field situation, and it thus requires further improvement.

For this reason, this paper proposes a non-contact voltage measurement method of near-end electric field inversion. Firstly, the principle of the near-end electric field inversion method is proposed by exploring the field source and electric field law, and deducing the relationship between the spatial electric field and voltage. Secondly, a three-phase conductor finite element simulation calculation model is established to obtain the spatial potential distribution under the three-phase horizontal arrangement, and the voltage inversion and calculation are performed on the electric field modulus obtained from the simulation results. Finally, an experimental platform for voltage measurement of a 10 kV overhead line was constructed, and the proposed near-end electric field inversion voltage measurement method was experimentally verified via a MEMS electric field sensor.

2. Proximal Voltage Inversion

2.1. Analysis of Relationship between Field Source and Electric Field

The core element of electromagnetic theory is Maxwell's system of equations, which consists of four main equations, from which it can be seen that the charged conductor is the source of the vector electric field [27]. When the voltage of the overhead line is in a steady state, the electric field in space at this time can be approximated as a quasi-static field, and therefore has the nature of an electrostatic field. Further, based on the Helmholtz theorem, in a certain region, the vector field is mainly determined by the field source information and regional boundary conditions. Therefore, for the general charged conductor, its charge distribution or surface potential can be uniquely determined by the distribution of the electric field around it [28]. Ideally, it can be assumed that the charged conductor is placed in a set computational region, as shown in Figure 1.

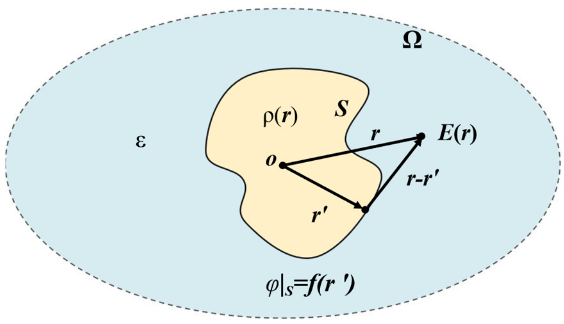

Figure 1. System structure diagram.

In Figure 1, Ω is the boundary of the calculation region; r is the position vector at the field point in the calculation region, and the potential on Ω is 0 when r tends to infinity [29]; r' is the position vector at the source point on the outer surface of the conductor; ε is the dielectric constant of the surrounding medium; S is the boundary of the outer surface of the charged conductor in the calculation region, which satisfies the first type of boundary conditions, i.e., $\varphi\,|_S = f(r')$, and $f(r')$ is the distribution function of the conductor's electric potential; $E(r)$ is the value of the electric field strength at any point r in the computational region.

The point position function at any location within the computational region satisfies the Poisson equation [28]:

$$\nabla^2 \varphi(r) = -\frac{\rho(r)}{\varepsilon} \tag{1}$$

Green's function $G(r, r')$ is introduced to solve Poisson's equation [30]. $G(r, r')$ is the solution of Poisson's equation for a given boundary condition in an electrostatic field and is defined as follows.

$$\nabla^2 G(r,\ r') = -\delta(r - r'), \tag{2}$$

The δ function in the above equation is defined as in Equation (3):

$$\begin{gathered} \delta(r - r') = \begin{cases} 0, & r \neq r' \\ \infty, & r = r' \end{cases} \\ \int_V \delta(r - r') dV = 1,\ r' \in V. \end{gathered} \tag{3}$$

Bringing $\varphi(r')$ and $G(r, r')$ into Green's second formula yields:

$$\varphi(r) = \int_\Omega \frac{\rho(r')}{\varepsilon} G(r,\ r') d\Omega + \varepsilon \int_S [G(r,\ r') \frac{\partial \varphi(r')}{\partial n'} - \varphi(r') \frac{\partial G(r,\ r')}{\partial n'}] dS, \tag{4}$$

The constructed Green function satisfies the following boundary conditions for the first type of boundary condition:

$$G(r,\ r') = 0,\ while\ r'\ is\ on\ S, \tag{5}$$

Equation (4) can be reduced to:

$$\varphi(r) = \int_\Omega \frac{\rho(r')}{\varepsilon} G(r,\ r') d\Omega - \varepsilon \int_S \varphi(r') \frac{\partial G(r,\ r')}{\partial n'} dS, \tag{6}$$

Bringing the first type of boundary conditions and $\rho(r') = 0$ into the above equation yields:

$$\varphi(r) = -\varepsilon \int_S f(r') \frac{\partial G(r,\ r')}{\partial n'} dS, \tag{7}$$

This can be obtained by considering the charged conductor to be solved as an equipotential body with potential φ_S:

$$f(r') = \varphi_S, \tag{8}$$

Equation (8) is obtained by substituting into Equation (7) and performing gradient operations in the r-direction on both sides of the equation:

$$-\nabla \varphi(r) = -\varepsilon \varphi_S \int_S \nabla \frac{\partial G(r,\ r')}{\partial n'} dS, \tag{9}$$

Order:

$$F(r) = \int_S \frac{\partial G(r,\ r')}{\partial n'} dS, \tag{10}$$

Combined with the electric field and potential relationship equation, Equation (11) can be obtained:

$$\varphi_S = \frac{1}{\varepsilon F(r)} \cdot E(r) \tag{11}$$

where ε is the dielectric constant of the surrounding medium and $F(r)$ is a constant when the regional boundary conditions are constant, indicating that the conductor potential φ_S is linearly related to its surrounding electric field $E(r)$. Therefore, through the electric field around the conductor, real-time sensing according to the linear proportionality between the electric field and the conductor voltage can provide the basis for the inversion of the conductor voltage.

2.2. Spatial Electric Field–Voltage Relationship

From the previous subsection, it is known that the electric field is linearly proportional to the voltage, so obtaining the proportionality coefficient is the key. In order to obtain $F(r)$ to establish an infinite length overhead line, the space electric field calculation model is shown in Figure 2.

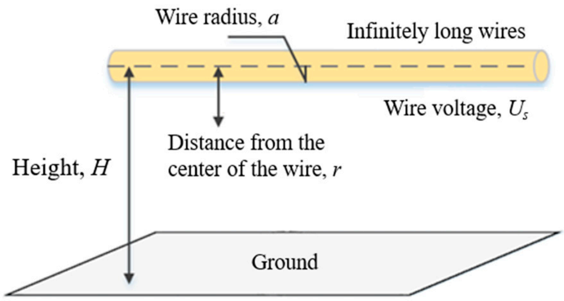

Figure 2. Space electric field calculation model of infinitely long overhead line.

In the figure, the single horizontal arrangement is taken as an example, the radius of the wire is a, the voltage is U_S, the height is H, the permittivity of the space around the wire is ε, the distance between any point below the wire and the center of the wire circle is r.

Let the charge per unit length of a charged wire be τ. Make a coaxial cylindrical closed surface S of radius r and height l a Gaussian surface, as shown in Figure 3.

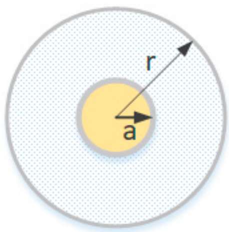

Figure 3. Gaussian surface for space electric field calculation.

According to Gauss's theorem:

$$\oint_S E \cdot dS = (2\pi rl)E = \frac{\tau l}{\varepsilon}, \tag{12}$$

$$E(r) = \frac{\tau}{2\pi r\varepsilon}, \tag{13}$$

$$U = -\int_H^r Edr = \frac{\tau}{2\pi\varepsilon} \ln \frac{H}{r} \quad a \leq r \leq \mathrm{H}. \tag{14}$$

In order to calculate the potential distribution below the dotted wire, as shown in Figure 4, for the ground $\varphi = 0$ boundary conditions, the mirror image method is used to deal with the space outside the point wire; that is, a wire with a unit length charge of $-\tau$ is placed in the mirror position with the ground as symmetry, the ground is removed, and the dielectric constant of the space below the ground and the space above the ground is ε.

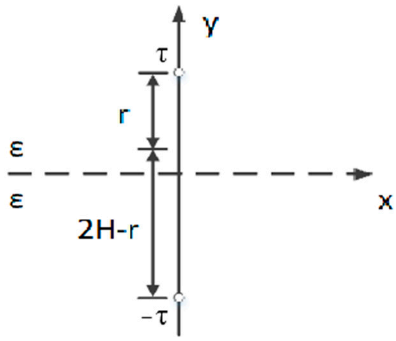

Figure 4. Transmission wire and mirror image.

The boundary problem corresponding to the method of mirroring the conductor with points is:

$$\nabla^2 \varphi = 0, \ Space\ outside\ the\ transmission\ wire, \tag{15}$$

$$\varphi|_S = 0, \ Ground. \tag{16}$$

The electric field above the ground is reduced to the sum of the electric field generated by the charge of the original transmission wire and the charge of the mirror line. According to $U|_{r=a} = U_S$, then:

$$U_S = \frac{\tau}{2\pi\varepsilon} \ln \frac{2H-a}{a} \quad a \le r \le H, \tag{17}$$

Substituting the above equation into the equation for $E(r)$ by eliminating τ, the electric field strength at the electric field measurement point below the wire can be obtained as:

$$E(r) = \frac{U_S}{r \ln(\frac{2H-a}{a})} \quad a \le r \le H, \tag{18}$$

Then, the following equation can be concluded:

$$U_S = E(r) r \ln(\frac{2H-a}{a}) \quad a \le r \le H. \tag{19}$$

Thus, via Equation (19) it is known that the voltage can be calculated by obtaining the value of the electric field.

2.3. Proximal Voltage Inversion Methods

In view of the inability of non-contact measurements to obtain the conductor body electric field, the concepts of near-source region and near region are proposed based on the linearization of the integration path via the existing electric field integration method, and are applied to the near-end electric field inversion method proposed in this paper. The overhead line is modeled and analyzed using COMSOL finite element simulation software, and a three-dimensional intercept line is set as the calculation path between the center of the conductor along the plumb line to the earth. The obtained electric field distribution is shown in Figure 5.

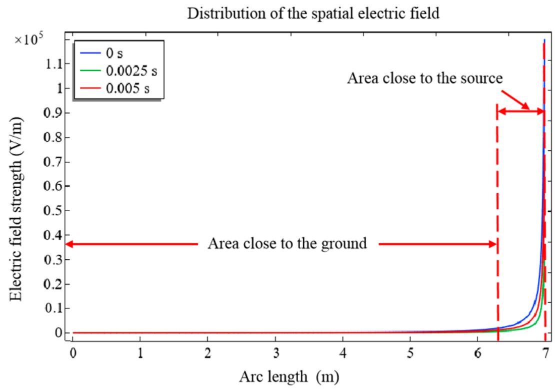

Figure 5. Electric field distribution under the intermediate phase conductor of overhead line.

From the figure, it can be seen that the electric field strength shows a decreasing law with the increase in the distance from the wire. It can also be seen that the value of the field strength is larger when it is close to the line neighborhood, while the electric field strength undergoes a sharp decrease when it exceeds a certain distance, when the field strength is smaller. Therefore, based on the above characteristics, two intervals can be defined for the electric field distribution area: the near-source area and the near area. In the near region, the electric field value tends to be stable, while in the near-source area, the electric field change rate is large and approximates a linear growth relationship. At this time, in the near-source area, through the collection of different distance conditions of the electric field value, and further use of linear fitting to obtain the conductor's electric field mode value, Formula (19) can be used to calculate the voltage value of the charged conductor, so as to ultimately realize the near end of the electric field of the non-intrusive contact voltage measurement.

3. Spatial Electric Field Simulation and Voltage Inversion

3.1. Three-Dimensional Simulation Model of Overhead Line

In this paper, COMSOL finite element simulation software is used to model the overhead line. In the process of building the model, the arc droop of the conductor is ignored and a limited number of long conductors are used to simulate the actual overhead transmission circuit. In the simulation model, the three-phase conductors are arranged horizontally and made of copper, and have a phase spacing of 0.5 m, a conductor radius of 0.016 m, a length of 2 m, and a height of 7 m. The voltage of the conductor is set to 10 kV, the ground voltage is set to 0 kV, the simulation time is set to be the two cycles of the standard sinusoidal waveform (0.04 s), and the step time is set to be 0.001 s. The points with different distances are set right below the center of the line, indicating the sensor measurement position., and the distance points indicate the measurement position of the sensor.

3.2. Potential Distribution of Overhead Lines

Figure 6 shows the 10 kV voltage level overhead line potential distribution diagram. Figure 6a shows, from left to right, for the A phase, B phase, and C phase, each phase voltage between each of the phases at 120°; Figure 6b–d show, for A, B, and C, the three-phase potential change law with time.

From Figure 6a, it can be seen that the conductor around the potential is large and, close to the ground, the potential gradually tends to zero, and the overhead line phase conductor below the electric field distribution law is consistent. From Figure 6b–d, it can be seen that, under different distance conditions of the voltage value and the conductor itself, the voltage change law is consistent and shows a certain proportionality. This is consistent with the results of the previous derivation.

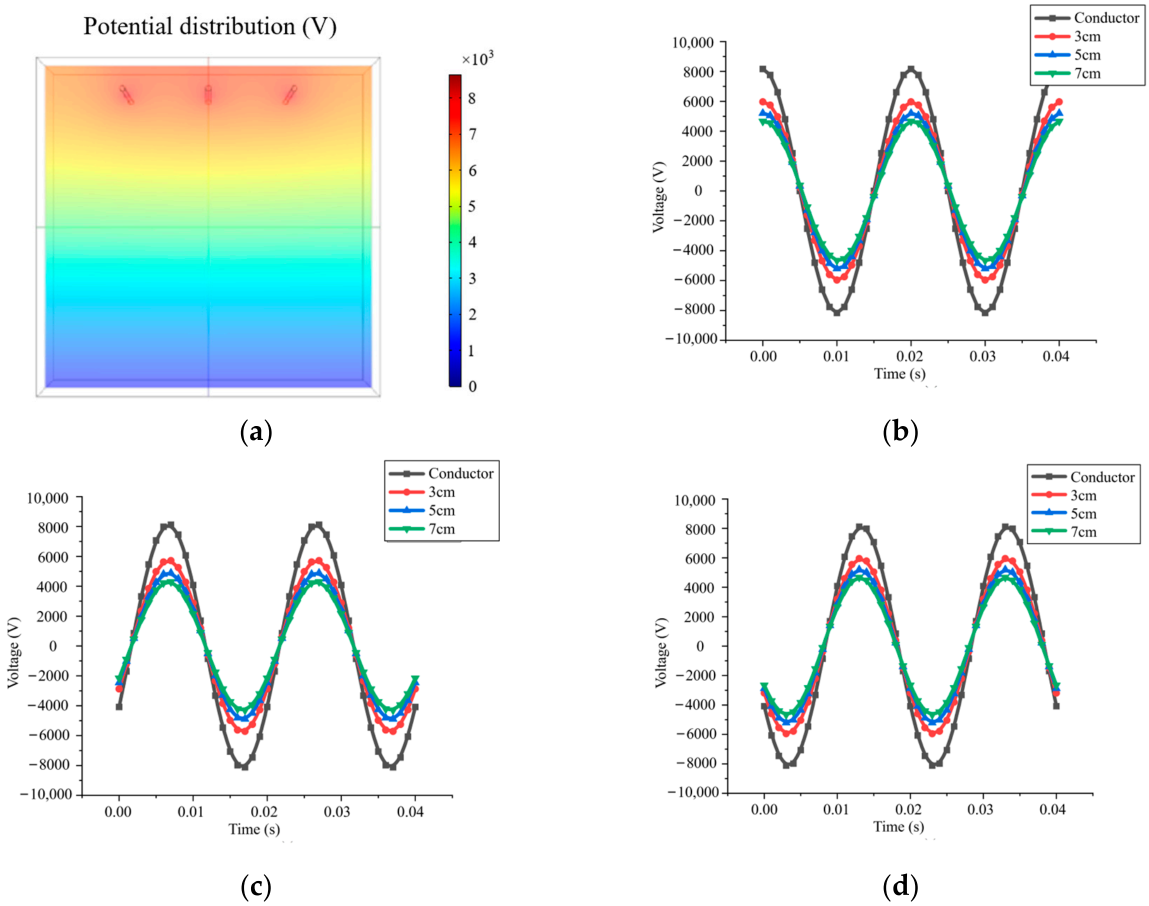

Figure 6. Potential distribution diagram of horizontal arrangement of overhead lines. (**a**) Overall spatial potential distribution. (**b**) A phase. (**c**) B phase. (**d**) C phase.

3.3. Voltage Inversion Calculation

Using Equation (19), the corresponding electric field values at different distances can be calculated, and these values are assumed to be theoretical values. Taking the radius of the center of the conductor as the reference point (i.e., at 0 cm), and 3 cm, 5 cm, and 7 cm from the conductor as the measurement points, the specific electric field values obtained are shown in Table 1.

Table 1. The electric field mode values calculated at different distance measurement points.

Distance (cm)	Electric Field Model Value (kV/m)
0	92.277
3	32.096
5	22.370
7	17.168

COMSOL finite element simulation software was further used to obtain the electric field modulus of phase A at different distances from the measurement point, and its change rule is shown in Figure 7.

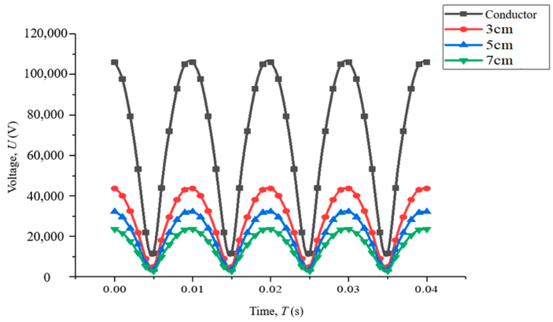

Figure 7. Variation rule of the electric field mode value of phase A.

From the figure, it can be seen that the electric field and the conductor space potential both show a sinusoidal change rule. In order to facilitate the comparative analysis, the electric field mode value when t is 0.01 s is selected and compared with the values in Table 1; it is obvious that the simulation results are larger than the theoretical calculation value. According to the principle of vector superposition of electromagnetic fields, considering that the A-phase electric field will be affected by the coupling from the B-phase and C-phase electric fields, the simulated electric field modulus is larger than the theoretical value. In order to compensate for the inverse effect of electric field coupling, the coupling scale factor k is introduced here.

$$k = \left| \frac{Simulation\ result - Theoretical\ value}{Simulation\ result} \right|. \tag{20}$$

The values in Table 1 and Figure 7 give a value of k of 0.129. In practical measurements, the electric field mode value of the conductor is obtained by linear fitting of the electric field mode value at the same voltage level and different distances. The simulation results can be read to obtain the fitting curve, as shown in Figure 8.

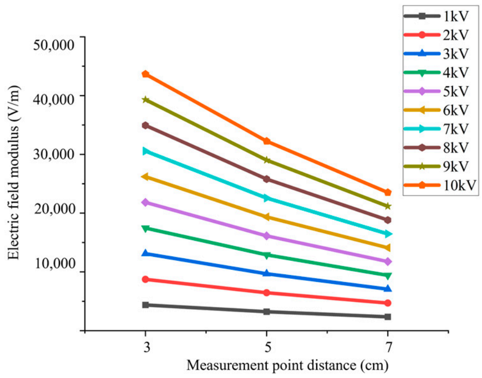

Figure 8. Linear fitting curve of electric field mode value.

From the figure, it can be seen that the slope between the two points closer to the conductor is also larger, which is consistent with the spatial electric field distribution law. At this point, via fitting, the electric field values obtained at the measurement points at different distances can be obtained when the distance is 0 cm. The corresponding space potential can then be iteratively obtained and the inverse voltage needs to take the coupling factor into account. The final U is:

$$U_{inverted\ voltage} = (1 + k) * U_{experiment\ voltage} \tag{21}$$

Therefore, according to the electric field modulus of the conductor obtained by fitting, via the resultant Equations (19) and (21) the voltage waveforms obtained by inversion are shown in Figure 9. From the figure, it can be seen that the inversion voltage is basically coincident with the reference voltage, in which the minimum error between the two is 0.5% and the maximum error is 6.8%. The results show that the non-contact measurement method of near-end electric field inversion voltage proposed in this paper can realize the high-precision measurement and calculation of the line.

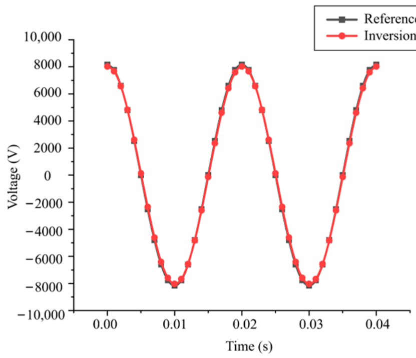

Figure 9. Voltage inversion results of the near-end electric field.

4. Experiments and Analysis of Results

4.1. Experimental Platform

At present, the sensors are developing in the direction of miniaturization and integration, and the non-contact and non-interference measurement of the device can be realized through the fusion of the sensor and the device co-morphism. Therefore, it is possible to apply the aforementioned proximal measurement principle to the on-line monitoring of the overhead line. Near-end measurement calculates the voltage by obtaining the near-end electric field data of the measured object. Therefore, it is crucial to accurately obtain the modal value of the electric field while taking into account the practicality of the monitoring device, so the size and volume of the sensor should not be ignored. The existing advanced MEMS electric field sensors can meet the above requirements and provide a good basis for practical applications. In order to comply with the harsh measurement point arrangement requirements of the existing electric field integration method, this paper proposes a concept to embed the sensor into a snap-on structure. This ultimately forms a non-contact voltage measurement system based on the proximal electric field inversion. The embedded structure includes the main control chip, wireless transmission, and energy supply module, in addition to the measurement (sensor) module, which is beyond the scope of this paper's investigation. Therefore, to realize the implementation of the above near-end measurement scheme, the overhead line simulation test platform is designed as shown in Figure 10.

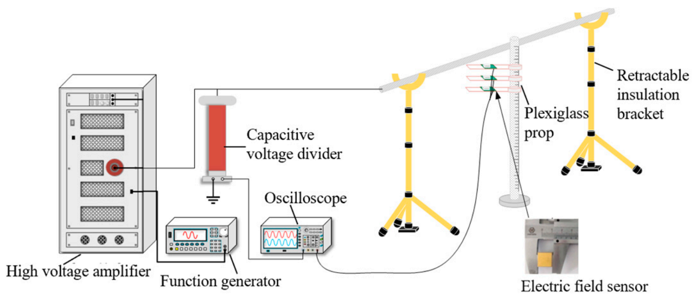

Figure 10. Overhead line simulation test platform.

Through the arbitrary function waveform generator and high-voltage amplifier placed in series, the amplified voltage is applied to the metal bar conductor through the high-voltage arm of the voltage divider capacitor, of which the arbitrary function waveform generator model is AFG3011. This model can generate 12 kinds of standard waveforms, as well as arbitrary waveforms of the voltage signal, and its output voltage can cover

40 mV–40 V, with the minimum adjustable scale of 1 mV. The high-voltage amplifier model is Model 50/12, the magnification is 5000 times, the bandwidth is DC ~1.5 kHz, and the maximum output voltage peak is 50 kV. It is used with an arbitrary function waveform generator to meet the test requirements of measuring periodic signals with high-amplitude voltages. The ratio of the high-voltage arm to the low-voltage arm of the partial voltage capacitor is 371:1. The metal rods have a radius of 8 mm and a length of 3 m, and the rods are mounted on a retractable insulating bracket. A torsional MEMS electric field sensor based on a piezoelectric drive was used to measure the electric field strength below the plumb line of the metal rod. The sensitivity of the MEMS electric field sensor is 3.24 mV/(kV/m), the measurement error is up to 3.75%, and the upper limit of the measurement frequency is 1 kHz. The electric field sensor is powered by a +5 V supply. The sensor was placed on the Plexiglas prop with a scale, and a fixture was used to change the distance between the sensor and the metal rod. The oscilloscope receives two signals: one signal is taken from the low-voltage arm of the voltage divider capacitor, which is used as a reference quantity, and the other comes from the measurement signal of the sensor. The oscilloscope model is a TDS2004C with four sampling channels, which has a bandwidth of 70 MHz and a sampling rate of 1.0 GS/s. The oscilloscope is used for the measurement of the sensor.

4.2. Analysis of Results

Considering the field environment of the high-voltage laboratory, the test height of the experiment in this paper is 2 m. Firstly, the MEMS electric field sensors are placed at the heights of 3 cm, 5 cm, and 7 cm from the conductor, and the position between the sensors and the conductor is adjusted to ensure that the sensors are directly underneath the conductor to obtain the plumb line direction electric field. During the experiment, the step-by-step voltage boosting method was used to boost the voltage to 10 kV in steps of 1 kV, and after the completion of each group of tests, the control variable method was utilized to change the distance between the sensor and the conductor. The aforementioned boosting method was then repeated. The output–input relationship of the sensors under different variable conditions and the output waveforms of the MEMS electric field sensors at different distances from the measurement point were finally obtained, as shown in Figures 11 and 12, respectively.

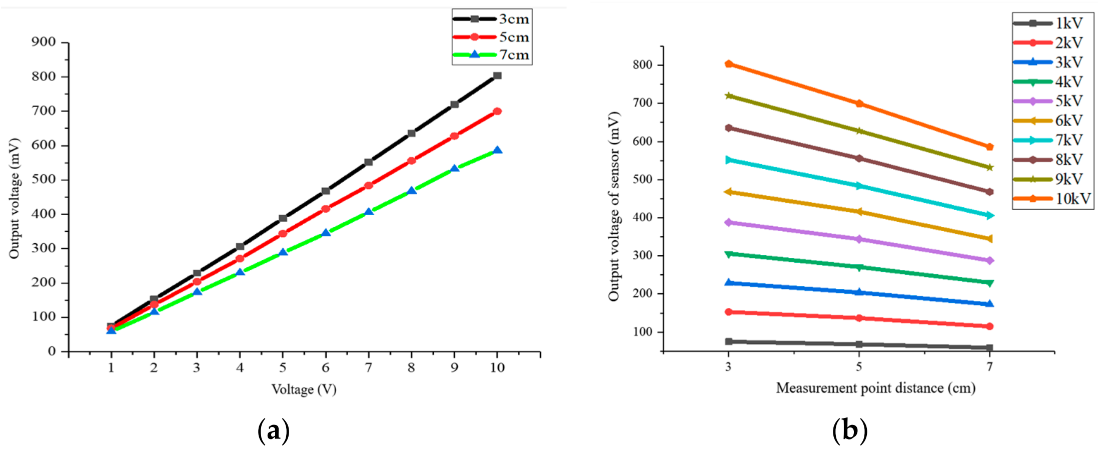

Figure 11. Relation between sensor output and input under different variable conditions. (**a**) Output of sensor at different voltage levels. (**b**) Output of sensor at measurement points in different distances.

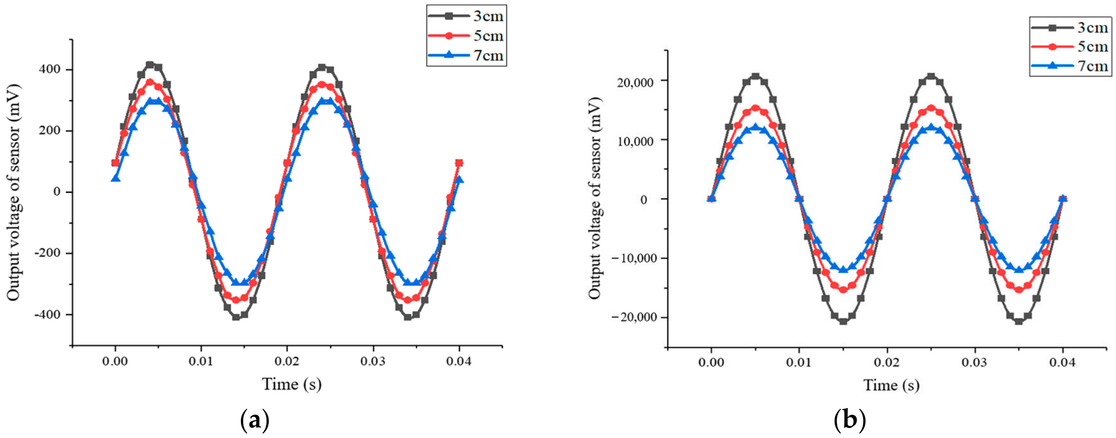

Figure 12. Output waveform of MEMS electric field sensor at different distance measurement positions. (**a**) Output voltage waveform of electric field sensor. (**b**) Electric field waveform corresponding to the electric field sensor.

From Figure 11a, it can be seen that, under the condition of keeping the distance of the measuring point unchanged, with the increase in the voltage level, the corresponding output of the sensor shows a linear change; at the same time, the closer to the measuring point of the electrically charged conductor, with the increase in the input voltage, the sensor's output increase is also greater. Figure 11b shows that the sensor measuring point is closer to the charged conductor. The sensor output value is also larger, and the slope between two adjacent points and the measuring point, and the distance between the earth, is directly proportional to the distance from the earth; the farther from the earth, the greater the slope. This not only follows the conductor electric field distribution law, but also reflects the linear proportionality between the electric field and voltage.

From Figure 12, it can be seen that, with the increase in the spacing between the sensor and the conductor, the sensor obtaining the output voltage value and the corresponding electric field value appears to experience a certain degree of reduction. At the same time, the output voltage waveform of the MEMS electric field sensor and the corresponding electric field waveform following the effect is good, and the same the rule of law is maintained.

The electric field data obtained by the sensor at different distances from the measurement point are substituted into the proximal electric field inversion algorithm to obtain the voltage of the conductor. The voltage waveform calculated by the inversion and the reference voltage waveform obtained by the voltage divider are shown in Figure 13.

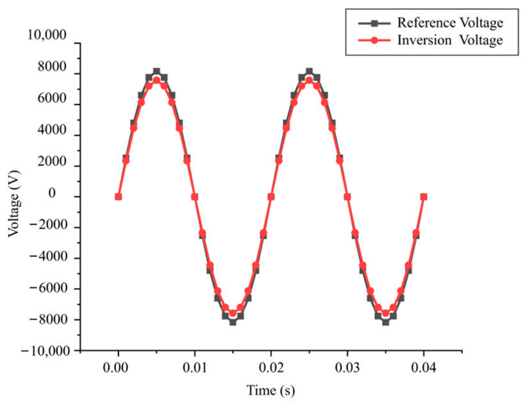

Figure 13. Comparison between inverse calculated line voltage waveform and actual voltage.

From the figure, it can be seen that the inverted voltage waveform through the near-end electric field basically coincides with the reference voltage waveform, and the maximum magnitude error between the two is 7.2%. The error may be due to three main factors: firstly, the systematic error of the MEMS electric field sensor itself; secondly, the accidental error caused by the inaccurate arrangement of the measurement points; and, finally, the fluctuation in the measured value during the data acquisition process. However, through repeated tests, the resultant errors caused by the above factors are within the acceptable range, and the experimental results can verify the accuracy and reliability of the non-contact voltage measurement method based on near-end electric field inversion proposed in this paper.

5. Discussion

1. By analyzing the field source law, the relationship between the space electric field and voltage is deduced, and the characteristics of linear proportionality between voltage and the electric field are obtained. This paper proposes a non-contact measurement method using the inverse voltage of the near-end electric field based on the above characteristics and the characteristics of the rate of change in the space electric field.
2. The three-phase conductor was modeled using finite element simulation software, and the space potential distribution characteristics below the plumbline of the three-phase conductor were obtained, which were consistent with the theoretical calculation of the electric field law. The simulation results show that the maximum error is 6.8%, which verifies the linear proportionality between the spatial electric field and the voltage of the conductor.
3. A simulation test platform of a 10 kV overhead line was built, and the electric field value under the conductor was measured using MEMS electric field sensors. The test results show that the error between the inversion voltage value and the actual voltage is 7.2%, which effectively proves the accuracy of the line voltage inversion method based on the near-end electric field measurement proposed in the paper.

The non-contact voltage measurement method based on proximal electric field inversion proposed in this paper provides new ideas for solving the problems of practical application difficulties due to the deficiencies in solving the electric field inverse problem and in the existing electric field integration method under the premise of ensuring the voltage measurement accuracy. At the same time, it is proposed to use existing advanced miniature electric field sensors and electrical equipment in a co-conformal and co-integrated manner in order to realize the non-contact voltage measurement of overhead lines. Finally, the research results of this paper can lay the foundation and provide guidance methods for engineering applications.

Author Contributions: Conceptualization, Q.Y. and K.K.; methodology, Q.Y. and K.K.; validation, S.S. and Z.Q.; formal analysis, F.M. and K.K.; investigation, H.N. and K.K.; resources, T.B. and Z.Q.; data curation, K.K. and Z.Q.; writing—original draft preparation, S.S. and Q.Y.; writing—review and editing, Q.Y.; supervision, Q.Y., K.K. and S.S.; project administration, F.M. and K.K.; funding acquisition, S.S. All authors have read and agreed to the published version of the manuscript.

Funding: This research was funded by State Grid Ningxia Electric Power Co., Ltd. Science and Technology Project Foundations of China, grant number 5229DK230005.

Data Availability Statement: Not applicable.

Conflicts of Interest: The authors declare no conflict of interest.

References

1. Yu, Y.; Zhao, K.; Ji, Z.; Li, C. Optimization setting method for simulation charge in wire in electric field calculation of transmission line. *Sci. Technol. Eng.* **2019**, *19*, 206–212.
2. Jiang, J.; Shen, J.; Huang, G.; Jin, T.; Tang, M.; Wang, J. Calculation and analysis of 220 kV transmission line power frequency electromagnetic field. *Sci. Technol. Eng.* **2022**, *22*, 13787–13793.
3. Yang, Q.; Dong, F.N.; Luo, M.D.; Sun, J.; Cui, H.; Jie, Q. Wideband Voltage Sensing Methods and Sensing Data Applications. *High Volt. Eng.* **2021**, *47*, 1969–1983. [CrossRef]
4. Zhang, Z.; Li, K.; Liu, J.; Jia, B.; Wang, P. Live detection technology of deteriorated insulator based on unmanned aerial vehicle inspection platform. *Sci. Technol. Eng.* **2019**, *20*, 8616–8621.

5. Han, Z.; Hu, J.; Li, L.; He, J. Process of Micro Electric Field sensing technology for new Power system. *Proc. CSEE* **2023**, *43*, 399–415.
6. Zhang, W.; Yang, Y.; Zhao, J.; Huang, R.; Cheng, K.; He, M. Research on a non-contact multi-electrode voltage sensor and signal processing algorithm. *Sensors* **2022**, *22*, 8573. [CrossRef]
7. Chen, K.L.; Guo, Y.; Ma, X.Y. Contactless voltage sensor for overhead transmission lines. *IET Gener. Transm. Distrib.* **2018**, *12*, 957–966. [CrossRef]
8. Yang, P.; Wen, X.; Lv, Y.; Chu, Z.; Peng, C. A non-intrusive voltage measurement scheme based on MEMS electric field sensors: Theoretical analysis and experimental verification of AC power lines. *Rev. Sci. Instrum.* **2021**, *92*, 65002. [CrossRef]
9. Luo, M.; Yang, Q.; Dong, F.; Chen, N.; Liao, W. Miniature Micro-Ring Resonator Sensor with Electro-Optic Polymer Cladding for Wide-Band Electric Field Measurement. *J. Light. Technol.* **2022**, *40*, 2577–2584. [CrossRef]
10. Hou, J.; Wu, G.; Cui, Y.; Zhao, L.; Li, Y. Modeling and Simulation Analysis of Silicon-based Miniature Electrostatic Resonant DC Electric Field Sensor. *Proc. CSEE* **2021**, *41*, 374–382+426.
11. Haberman, M.A.; Spinelli, E.M. A Noncontact Voltage Measurement System for Power-Line Voltage Waveforms. *IEEE Trans. Instrum. Meas.* **2020**, *69*, 2790–2797. [CrossRef]
12. He, W.; Yang, F.; Yao, D. Application of simulated charge method to solve the inverse problem of insulator electric field and on-line monitoring of inferior insulators. In Proceedings of the 9th National Electrical and Mathematical Academic Annual Conference, Ning'an, China, 1 September 2003.
13. Yang, F. Forward and Inverse Problems of Power Frequency Electric Field and Electromagnetic Environment of Power Transmission and Transformation Equipment. Ph.D. Thesis, Chongqing University, Chongqing, China, 1 April 2008.
14. Yu, M.; Wang, J.; Wen, S.; Xiong, L. Research on the Non-contact Charge Induction Potential Transformer Based on Inverse Problem of Electric Field. *Electr. Meas. Instrum.* **2012**, *49*, 82–85+90.
15. Gao, C.; Wang, J.; Fan, Y.; Zhu, L. Experiment and research of voltage sensor of high-voltage transmission line based on inversion problem of electric Field. *Power Syst. Prot. Control* **2014**, *42*, 99–104.
16. Gao, C.; Wang, J.; Yang, J.; Peng, H.; Ma, J. Experiment and Simulation of D-dot Voltage Probe Based on Inverse Problem of Electric Field. *Trans. China Electrotech. Soc.* **2016**, *31*, 36–42.
17. Wang, J.G.; Zhao, P.C.; Wang, Q.; Zhou, M.; Huang, H. Research on Dual-differential D-dot Overvoltage Sensor Based on the Inverse Problem of Electric Field. *Proc. CSEE* **2020**, *40*, 5363–5373. [CrossRef]
18. Xiao, D.P.; Xie, Y.T.; Liu, H.T.; Ma, Q.; Zheng, Q.; Zhan, Z. Position optimization of measuring points in voltage non contact measurement of ac overhead transmission lines. *Appl. Comput. Electromagn. Soc. J.* **2017**, *32*, 908–914.
19. Xiao, D.; Xie, Y.; Ma, Q.; Zheng, Q.; Zhang, Z. Non-contact voltage measurement of three-phase overhead transmission line based on electric field inverse calculation. *IET Gener. Transm. Distrib.* **2018**, *12*, 2952–2957. [CrossRef]
20. Yang, M.; Xiong, Z.; Sima, W.; Li, Y.; He, D.; Zou, B. Solution of the Inverse Problem of "Low-Frequency Overvoltage Excitation to Response" for Electromagnetic Potential Transformers. *Trans. China Electrotech. Soc.* **2021**, *36*, 3605–3613.
21. Rahmatian, F.; Chavez, P.; Jaeger, N. 230 kV optical voltage transducers using multiple electric field sensors. *IEEE Trans. Power Deliv.* **2002**, *17*, 417–422. [CrossRef]
22. Chavez, P.P.; Jaeger, N.; Rahmatian, F. Accurate voltage measurement by the quadrature method. *IEEE Trans. Power Deliv.* **2003**, *18*, 14–19. [CrossRef]
23. Zhu, Y.; Ye, M.Y.; Liu, J.; Luo, S.N.; Xu, Y.; Yi, T. Design of 220 kV Combined Optical Voltage and Current Transformer. In Proceedings of the 4th National Intelligent Electrical Equipment and Its Application, Yantai, China, 1 November 2000.
24. Wang, J.G.; Yan, X.J.; Zhong, L.; Zhu, X.B. Simulation and Test of a Contactless Voltage Measurement Method for Overhead Lines Based on Reconstruction of Integral Node Parameters. *Sensors* **2020**, *20*, 246. [CrossRef] [PubMed]
25. Yan, X.; Wang, J.; Zhao, P.; Shen, Z.; Li, X.; Zhang, R. Design and Test of Contactless Overvoltage Sensor With Spherical Six-Electrode. *IEEE Trans. Instrum. Meas.* **2021**, *70*, 9508511. [CrossRef]
26. Wang, J.; Yan, X.; Li, X.; Liao, J.; Tao, Y. Method and Experimental Study of Transmission line Voltage Measurement Based on a Gauss-Type integral Algorithm. *Trans. China Electrotech. Soc.* **2021**, *36*, 3978–3986.
27. Yan, X.; Wang, J.; Shen, Z.; Zhao, P.; Li, X.; Wang, Q. A Self-decoupling Contactless Overvoltage Measurement Method Based on Optimization of Measuring Point. *IEEE Trans. Instrum. Meas.* **2022**, *71*, 1002711. [CrossRef]
28. Ma, X. *Electromagnetic Field Theory and Applications*; Xi'an Jiaotong University Press: Xi'an, China, 2000.
29. Guo, F.; Ma, S. Finite Element Method Combined with Asymptotic Boundary Condition Technique for Solving the Problem of Unbounded Planar Electrostatic Field. *High Volt. Appar.* **1997**, *33*, 20–24.
30. Hu, X. On the Basic Method of Solving Linear nonhomogeneous Mathematical Physics Equations in Unbounded Space with Green Function. *J. Chongqing Norm. Univ. (Nat. Sci. Ed.)* **1987**, *00*, 65–75.